CAMBRIDGE
UNIVERSITY PRESS

Research Paper

The capability of the Australian Square Kilometre Array Pathfinder to detect prompt radio bursts from neutron star mergers

Ziteng Wang[1,2,3], Tara Murphy[1,3], David L. Kaplan[4], Keith W. Bannister[2] and Dougal Dobie[1,2,3]

[1]Sydney Institute for Astronomy, School of Physics, University of Sydney, Sydney, New South Wales 2006, Australia, [2]CSIRO Astronomy and Space Science, PO Box 76, Epping, New South Wales 1710, Australia, [3]ARC Centre of Excellence for Gravitational Wave Discovery (OzGrav), Hawthorn, Victoria, Australia and [4]Center for Gravitation, Cosmology, and Astrophysics, Department of Physics, University of Wisconsin-Milwaukee, P.O. Box 413, Milwaukee, WI 53201, USA

Abstract

We discuss observational strategies to detect prompt bursts associated with gravitational wave (GW) events using the Australian Square Kilometre Array Pathfinder (ASKAP). Many theoretical models of binary neutron stars mergers predict that bright, prompt radio emission would accompany the merger. The detection of such prompt emission would greatly improve our knowledge of the physical conditions, environment, and location of the merger. However, searches for prompt emission are complicated by the relatively poor localisation for GW events, with the 90% credible region reaching hundreds or even thousands of square degrees. Operating in fly's eye mode, the ASKAP field of view can reach $\sim 1\,000$ deg^2 at $\sim$888 MHz. This potentially allows observers to cover most of the 90% credible region quickly enough to detect prompt emission. We use skymaps for GW170817 and GW190814 from LIGO/Virgo's third observing run to simulate the probability of detecting prompt emission for GW events in the upcoming fourth observing run. With only alerts released after merger, we find it difficult to slew the telescope sufficiently quickly as to capture any prompt emission. However, with the addition of alerts released *before* merger by negative-latency pipelines, we find that it should be possible to search for nearby, bright prompt fast radio burst-like emission from GW events. Nonetheless, the rates are low: we would expect to observe $\sim$0.012 events during the fourth observing run, assuming that the prompt emission is emitted microseconds around the merger.

Keywords: gravitational waves – radio continuum: general – methods: observational

1. Introduction

In 2017, the Advanced Laser Interferometer Gravitational-Wave Observatory and Virgo Interferometer (aLIGO/Virgo; Aasi et al. 2015; Acernese et al. 2014) detected gravitational waves (GWs) from a binary neutron star (BNS) merger, GW170817 (Abbott et al. 2017a), followed by the detection of gamma rays 1.7 s later (GRB 170817A; Abbott et al. 2017b). It was the first joint detection of GWs and electromagnetic radiation from the same source. However, the delay in issuing the alert and large error region prevented most telescopes from searching for any prompt transient event microseconds around the merger.

Many models (including some that predate the discovery of fast radio bursts (FRBs; Lorimer et al. 2007; Thornton et al. 2013; Cordes & Chatterjee 2019)) predict prompt radio emission associated with compact object mergers. This emission could be generated by the magnetic field interactions during the inspiral (Hansen & Lyutikov 2001; Lai 2012; Totani 2013; Metzger & Zivancev 2016; Wang et al. 2016, 2018), interaction between a relativistic jet and interstellar medium (Pshirkov & Postnov 2010), or the collapse of a supramassive neutron star remnant into a black hole (Ravi & Lasky 2014; Falcke & Rezzolla 2014).

In particular, prompt emission may be in the form of short coherent radio pulses like FRBs. While some estimates suggested that neutron star mergers could not be the sole progenitors of FRBs because the volumetric rate of FRBs is significantly higher than that of BNS mergers, $\gtrsim 10^4$ Gpc^{-3} yr^{-1} (Ravi 2019; Cao, Yu & Zhou 2018) versus 1540^{+3200}_{-1220} Gpc^{-3} yr^{-1} (Abbott et al. 2017b, also see Callister, Kanner, & Weinstein 2016), other estimates of the FRB rate have found better agreement (Lu & Piro 2019). However, the detection of repeating FRBs (e.g., FRB121102 Spitler et al. 2016) clearly demonstrates that not all FRBs originate from BNS mergers. Further complications have come from recent observations, when the Galactic magnetar SGR 1935+2154 had X-ray outbursts (Mereghetti et al. 2020a, 2020b; Ridnaia et al. 2020a, 2020b ; Zhang et al. 2020) accompanied by simultaneous radio bursts (Scholz & Chime/Frb Collaboration 2020) of a brightness consistent with faint extragalactic FRBs (Bochenek et al. 2020; Margalit et al. 2020). James et al. (2019b), Macquart & Ekers (2018), and James et al. (2019a) also note that the FRB distribution we have got so far may be different by taking statistical and systemic effects into account. As it stands, the fraction of non-repeating FRBs potentially caused by BNS mergers is unclear, but a single discovery would change that. Furthermore, the detection of prompt emission from a BNS merger would be a useful tool to measure the interstellar medium and magnetic environment (Lu, Kumar, & Narayan 2019) near the merger and locate the progenitor quickly, going from the 10–1 000 deg^2 localisation from GW alone (Singer et al. 2014; Abbott et al.

2020) to ∼arcmin (Bannister et al. 2017) for FRBs localised by the Australian Square Kilometre Array Pathfinder (ASKAP; Johnston et al. 2008). Combining this localisation with distance constraints from GW pipelines may be sufficient to uniquely identify a host galaxy, even in the absence of sub-arcsecond localisation.

The timing of radio emission relative to the merger varies between different models. Totani (2013) predicts that FRBs produced by the magnetic field interactions could occur milliseconds before the BNS merger, while Falcke & Rezzolla (2014) predict an FRB due to the collapse of the supramassive neutron star produced 10–10 000 s after the merger. Hence to detect or put limits on this prompt emission, we need to cover the GW error region as quickly as possible, ideally before the merger occurs, and then continue observing for minutes to hours after.

In late 2021, a four-detector GW network with the two aLIGO instruments, aLIGO Hanford (H) and aLIGO Livingston (L) combined with Phase 1 of Advanced Virgo (V) and the Kamioka Gravitational Wave Detector (KAGRA, or K; Somiya 2012; Aso et al. 2013) will be online for the fourth GW observing run (O4; Abbott et al. 2018), with BNS detectability ranges from 160–190 Mpc (L, H) to 90–120 Mpc (V) to 25–130 Mpc (K). During O4, the network is expected to detect between 3 and 110 BNS mergers using the estimated BNS event rate of 110–3 840 $Gpc^{-3} yr^{-1}$ scaled from the observation of GW170817 (Abbott et al. 2019).

In contrast to O3 and earlier, where GW alerts were released only after the mergers with latencies of minutes to hours, in the O4 observing period it is expected that at least one negative-latency pipeline will be operating on the LHVK network. Negative-latency pipelines use matched filters to detect GW signals in the inspiral phase, which enables an alert to be released before the BNS merger occurs (Cannon et al. 2012; Chu et al. 2016). James et al. (2019b) illustrated that summed parallel infinite impulse response (SPIIR; Hooper et al. 2012a, 2012b) can detect GW170817-like events about 30 s before the merger with detection signal-to-noise ratio (SNR) of ∼10. Chu et al. (2016) found that the median localisation error areas can be better than 500 deg^2 with a four-detector network 40 s before the coalescence.

There have been several unsuccessful attempts to search for prompt radio emission from compact binary coalescence at low radio frequencies. Callister et al. (2019) used the Owens Valley Radio Observatory Long Wavelength Array (OVRO-LWA, observing at 27–85 MHz)[a] to search for the prompt emission from the binary black hole merger GW170104, while Anderson et al. (2018) used the OVRO-LWA to search for prompt emission from the cosmological short gamma-ray burst 170112A. Similarly, Rowlinson & Anderson (2019) examined data (Kaplan et al. 2015) from the Murchison Widefield Array (MWA; Tingay et al. 2013, observing at 70–300 MHz) from the short gamma-ray burst 150424A. However, these events are well beyond the BNS detection sensitivity distance in O4 ($z \sim 0.05$). More broadly, Kaplan et al. (2016) investigated strategies to observe prompt emission from GW events with the MWA (also see James et al. 2019b).

The Australian Square Kilometer Array Pathfinder (ASKAP; Johnston et al. 2008) is a 36×12-m antenna radio telescope located in Western Australia, operating over the frequency range 700 MHz to 1.8 GHz. In 2019, we conducted follow-up observations of several GW events with ASKAP in its standard imaging mode (e.g., Dobie et al. 2019b). In parallel, the Commensal Real-time ASKAP Fast Transients (CRAFT) survey Macquart
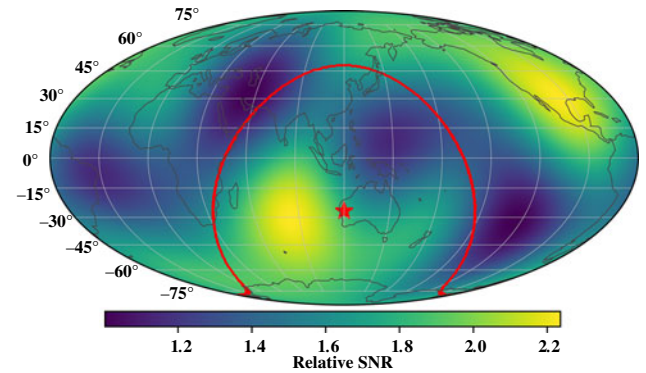

Figure 1. Sensitivity map of the gravitational wave detector network in O4 (HLVK). The colour is proportional to the relative signal-to-noise ratio. The red line shows the ASKAP horizon (15° in elevation angle) and the red star is where ASKAP is located.

et al. 2010) has developed high time resolution (1 ms) capabilities on ASKAP, which has resulted in the discovery of at least 32 FRBs (e.g., Shannon et al. 2018; Bannister et al. 2017; 2019). The localisation precision for ASKAP can be ∼arcminute with probabilistic localisation techniques (e.g., Bannister et al. 2017), going to ∼arcsecond using standard interferometry techniques (e.g., Bannister et al. 2019). ASKAP covers sky regions of a higher detection sensitivity for the GW detector network than some other radio telescopes (we show the corresponding sensitivity map in Figure 1). This enables ASKAP to detect GW signals earlier. However, the differences will be smaller in the future with more detectors joining the network.

In this paper, we discuss the capabilities of ASKAP for detecting prompt emission from GW events.

2. Negative-latency pipelines

There are a number of pipelines running on aLIGO/Virgo that are designed to rapidly identify compact binary merger events. The key pipelines are GstLAL (Messick et al. 2017; Sachdev et al. 2019), multi-band template analysis (MBTA; Adams et al. 2016), PyCBC Live (Dal Canton & Harry 2017; Nitz et al. 2018), and SPIIR (Hooper et al. 2012a, 2012b).

Each pipeline sends an alert to the Gravitational-Wave Candidate Event Database (GraceDB)[b] if the detection statistic (e.g., SNR) of the candidate passes a predetermined threshold. In order to collect the information about a single physical event in one place and issue a single alert per physical event, GraceDB gathers individual alerts into a 'superevent' data model.[c] Pipelines which send out superevents quickly will facilitate searches for prompt emission from BNSs.

Bayesian triangulation and rapid localisation (BAYESTAR; Singer & Price 2016) algorithms can offer observers a rapid parameter estimation for the GW events including the event localisation (e.g., Figure 2 for GW170817), distance, and component masses estimates. In general, increasing from a two-detector network to a three-detector network (O3) and to a four-detector network operating in O4 will improve localisation (e.g., Chu et al. 2016; Abbott et al. 2017b).

However, moving to a negative-latency search will reduce the SNR at detection and hence increase the location uncertainty. In

---

[a] http://www.tauceti.caltech.edu/LWA/.

[b] https://gracedb.ligo.org/.
[c] See https://gracedb.ligo.org/documentation/models.html#superevents and https://emfollow.docs.ligo.org/userguide/analysis/superevents.html.

Table 1. ASKAP antenna mount operating characteristics[a].

Axis	Range of motion	Rotation range	Slew rate	Acceleration/deceleration speed
Azimuth	Full	+/–270 deg	3 deg s^{-1}	3 deg s^{-2}
elevation	+15 deg to +89 deg	N/A	1 deg s^{-1}	1 deg s^{-2}

[a] From Australia Telescope National Facility (ATNF): https://www.atnf.csiro.au/projects/askap/ASKAP_Antenna_public_specification_Nov08_v0.0.pdf.

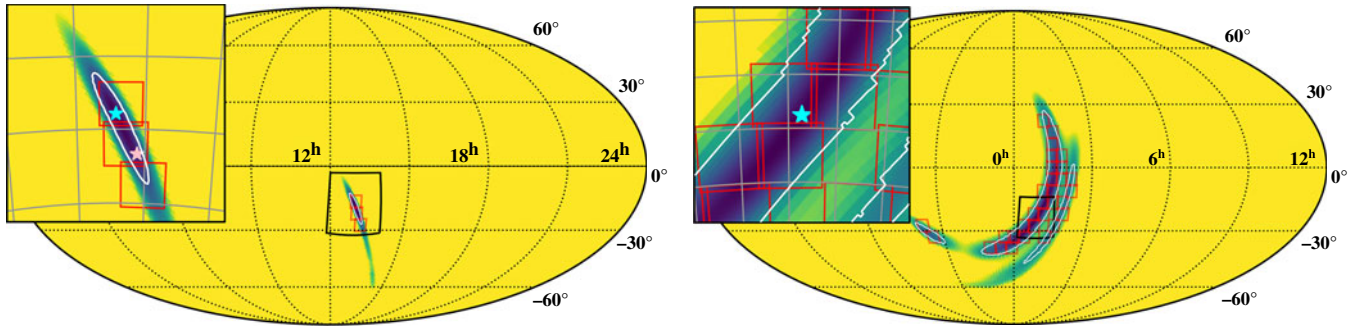**Figure 2.** Sky localisation maps for GW170817 (Abbott et al. 2017b; left) and the initial map for GW190814 (https://gracedb.ligo.org/apiweb/superevents/S190814bv/files/bayestar.fits.gz.) (Abbott et al. 2020; right). The colour is proportional to the $\log_{10}$ of the probability. Maps are plotted in equatorial coordinates using the Mollweide projection. The 90% credible regions are shown by the white lines. The optimised tilings of ASKAP (Dobie et al. 2019a) to cover 90% credible region are shown in the red squares. Each square is 6×6 deg^2 FoV of ASKAP. The number of ASKAP tilings for GW170817 is 3, while that for GW190814 is 35. The cyan star shows the position with the maximum posterior probability for both events and the pink star shows where GW170817 actually was. Zoomed regions show the insets around the maximum posterior probability positions. The sizes for zoomed regions are 30×30 deg^2 (left) and 20×20 deg^2 (right), respectively.

general, the earlier the detection is, the lower SNR the pipeline will determine and the worse the localisation the pipeline will produce (Chu et al. 2016). James et al. (2019b) shows that the SNR of the GW170817 signal at $t_0 - 30$ (i.e., 30 s before the merger at t_0) is one-third of that at the time of the merger. Cannon et al. (2012) and Chu et al. (2016) show that the localisation can be thousands of square degrees at $t_0 - 30$ s, even if it is less than 30 deg^2 at t_0. Chu et al. (2016) used simulated data to calculate the median 90% credible regions at different times prior to merger for different detector networks. The 90% credible region will improve from about 2 200 deg^2 to 1 600 deg^2 at $t_0 - 40$ s from O3 with the LHV network to O4 with the LHVK network.

3. ASKAP capabilities

ASKAP consists of 36 antennas which can point along their altitude and azimuth axes separately, with operating characteristics in Table 1. The telescope can slew at a rate of 3 and 1 deg sec^{-1} in azimuth and altitude, respectively. The rotation range for the azimuth axis is from $-270°$ to $270°$ to allow for cable wraps. When reaching one of these limits, the antennas may need to unwrap by $\pm360°$ even if the target position is very close to the starting position, adding an additional overhead of $\sim$120 s. ASKAP has an additional rotation axis where the dish rotates around the optical axis. In a typical fast-slew strategy, we would choose not to change the dish rotation in order to minimise the total settling time.

There are two operational modes for ASKAP to look for FRB-like emission[d]: collimated incoherent mode and fly's eye mode (Bannister et al. 2017, and see Table 2). In the collimated incoherent mode, all the antennas point in the same direction, and the total power detected at each antenna is combined incoherently. In the fly's eye mode, each antenna points in a different direction

Table 2. Sensitivity, field-of-view (FoV), and angular resolution for different ASKAP of sub-arrays.

Configuration	FoV[a] (deg^2)	σ_{det}^{b} (Jy)	Localisation capability
1-antenna sub-array	$\sim$1 080	2.4	$10' \times 10'$
36-antenna sub-array	$\sim$30	0.4	$3'' \times 3''$

[a] This assumes that we can use all 36 antennas and all antennas operate in the same configuration but different sub-array points to different positions.
[b] With integration time of 1 ms, bandwidth of 336 MHz.

and we can achieve a total field of view (FoV) N$\times$30 deg^2 with N antennas, albeit with reduced sensitivity.

There is also a mode between the collimated incoherent mode and fly's eye mode where one can use the 36 antennas in separate incoherent sub-arrays. For example, 36 antennas can be operated simultaneously as 6 separate 6-antenna arrays, with each sub-array producing a separate data stream. Fly's eye mode is equivalent to 1-antenna sub-arrays, while full collimated incoherent mode is corresponding to 36-antenna sub-array.

The detection uncertainty, σ_{det}, for a single ASKAP antenna is

$$\sigma_{\text{det}} = \frac{\text{SEFD}}{\sqrt{\Delta\nu t N_{\text{pol}}}}, \qquad (1)$$

where SEFD is the system equivalent flux density ($\sim$2 000 Jy for ASKAP)[e], $\Delta\nu = 336$ MHz is the bandwidth, t is the integration time, and $N_{\text{pol}} = 2$ is the number of the polarisations. Typical FRB searches use $t = 1$ ms. Using the equation above, the noise for a single ASKAP dish for an FRB search is roughly 2.4 Jy. When combining multiple antennas incoherently the noise decreases as $1/\sqrt{N_{\text{ant}}}$, with N_{ant} the number of antennas. Therefore, the noise can reach $\sim$ 0.4 Jy for the collimated incoherent mode when using all 36 antennas.

[d] As yet ASKAP cannot do a fully coherent FRB search using all antennas.

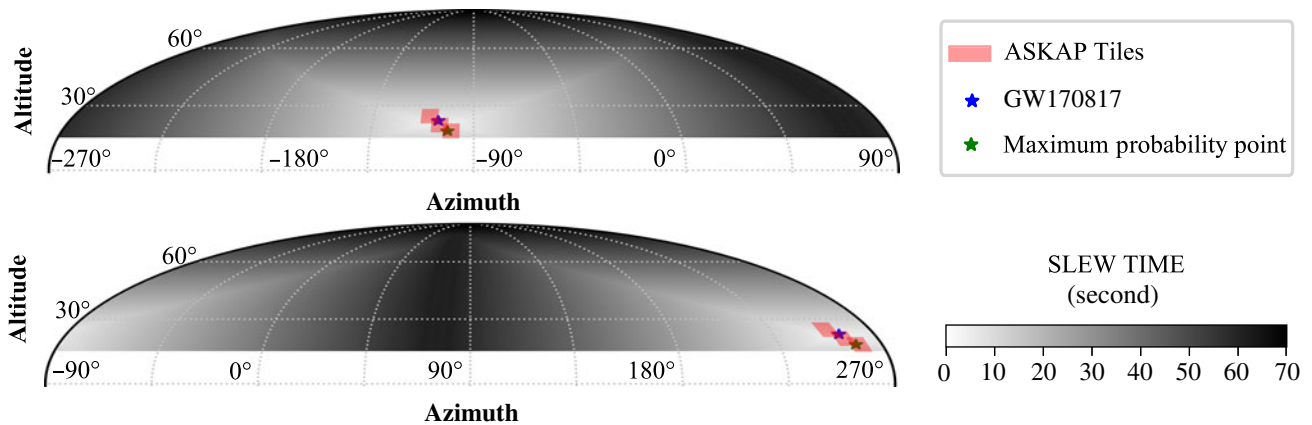[e] https://www.atnf.csiro.au/projects/askap/memo015_a.pdf.

Figure 3. Slew time (indicated by the grey scale) for different starting positions for GW170817 as a function of starting azimuth and altitude. The red rectangles show the tiling for the bayestar skymap from the HLV network. The blue star shows the point where GW170817 is and the green star shows the maximum probability position of the skymap. The figure is in the azimuth/altitude coordinates and is modified to cover azimuths from $-270°$ to $270°$, allowing for antenna motion over that range.

4. Slewing simulations

Most models predict that prompt emission (if present) would occur within a few seconds of the merger (e.g., Hansen & Lyutikov 2001). The chance of detecting this prompt emission will depend on both the latency of the pipelines and the slew time of the antennas. If the latency plus the slew time is smaller than the delay before radio emission, it may be possible to detect prompt emission.

Given initial and final positions of each antenna, we can use Table 1 to calculate the slew time for both axes (including acceleration and deceleration) and take the maximum of the two axis times as the slew time of each antenna. However, since we consider observation modes where all of the antennas end up pointing in different positions, we take the maximum of the slew times of all antennas as the slew time for the event.

We test this with two limiting cases: (1) a small event region where all of the antennas point to the same location (credible region $\lesssim$ ASKAP FoV) and (2) a large event region where we use the fly's eye mode to tile as much as we can. Since the starting positions are unknown, we simulate this with randomised starting positions but two concrete sky maps: GW170817 (Abbott et al. 2017b) as a small region ($\sim$30 deg^2), and GW190814 as a large region ($\sim$772 deg^2), as illustrated in Figure 2. We use the initial BAYESTAR skymap for GW190814 (LIGO Scientific Collaboration and Virgo Collaboration et al. 2019) as an example of a poor early-time localisation (although we note that the final LALInference skymap had a smaller 90% localisation of $\sim$30 deg^2 which was similar to that for GW170817). The 90% localisation in Figure 2 is significantly larger than the ASKAP FoV and is elongated (like most GW localisations) and therefore it serves as a useful illustration.

The starting conditions were randomised with equal probability for all azimuths and uniform in cosine of the elevation angle (equal probability per sky area) between 15° and 89°.

For the small region, GW170817 ($\sim$30 deg^2), we can cover the 90% credible region with three FoVs (shown in Figures 2 and 3). Figure 3 shows the spatial distribution of slewing time for GW170817. The median slewing time to get on-source is 40.3 s, with a range of 15.5–59.3 s for the 10th and 90th percentiles, respectively, as shown in Figure 4.
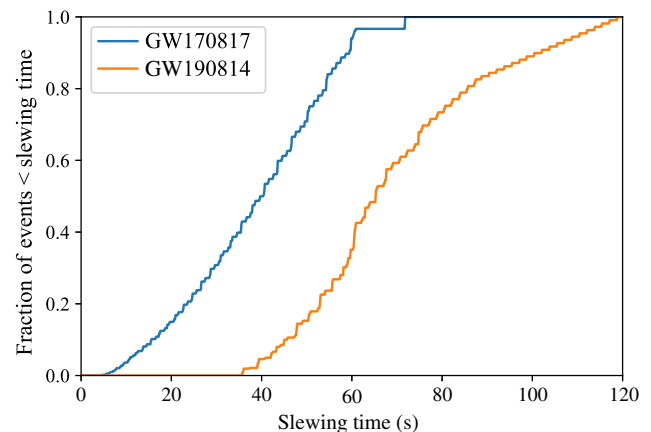

Figure 4. Cumulative histogram of slew times for GW170817 (blue) and GW190814 (orange) for different initial positions. The y-axis shows the fraction of the events whose slew time is smaller than the value on the x-axis.

For the large region, we used the strategy in Dobie et al. (2019a) to optimise the ASKAP pointing. For simplicity, we called the coverage of a single antenna tiling. This strategy optimises the tiling centre position to tile as much of the 90% credible region as ASKAP can. If more than the maximum 36 antennas are needed to tile the 90% credible region, then less area will be covered. However, if we can cover the 90% region with fewer than 36 antennas, then more than one antenna is pointed towards the highest probability region. We used the GW190814 bayestar localisation to perform our simulation for the large region. We need all 36 antennas to cover the 90% credible region. As is shown in Figure 3, the 50th and 90th percentiles slewing times to get on-source are 65.2 and 102.0 s.

5. Discussion

There could be as many as tens of BNS mergers detected by the HLVK GW detector network in the O4 run (Abbott et al. 2018). It may be impossible to follow up every event, especially including false alarms that increased during the low-latency portions of O3 and might increase further with negative latencies.

Only high signal-to-noise GW events will be amenable to negative-latency detections, such that the reduced signal-to-noise ratio will still pass the detection threshold. Overall, higher SNR detections lead to smaller localisations, with $A \propto (\rho \sigma_f)^{-2}$ where ρ is the SNR and σ_f is the effective bandwidth of the source in the detector (Fairhurst 2009). While high-ρ events will have well-localised detections eventually, moving to negative latency will reduce the instantaneous ρ and σ_f and therefore increase the sky area accordingly. At the threshold where $\rho \geq 8$ at $t_0 - 30$ s, the first localisation map would have an area of $\sim$ few $\times 10^3$ deg^2, decreasing to a few deg^2 for the final detection with $\rho \sim 25$ (Cannon et al. 2012).

We now examine how a likely scenario could play out for a prompt ASKAP search. The typical time for downloading the skymap and calculating the pointings is of the order of 1 s. We examine a nominal event occuring at a distance of $\sim$130 Mpc, with an early-warning $\rho = 8$ at $t_0 - 30$ s and a 90% localisation of $\sim 5\,000$ deg^2. This would imply a slew time of 60–90 s, similar to the GW190814 case in Section 4. The dispersion measure, induced by the intergalactic medium, of events at this distance is 363 pc cm^{-3} (James et al. 2019b) and therefore a time delay to an ASKAP frequency of 900 MHz of only 1.9 s. The time delay due to the intergalactic medium is relatively small compared to the slewing time, and in this case the time delay can be considered negligible ASKAP will therefore miss this event by $\gtrsim$1 min. However, we note that based on Figure 4, there are about 10% of events where the slew time will be $\sim$ 50 s, in which case we may be able to conduct a search for pre-merger prompt emission.

An ideal event for our search would have an early-warning sky area which is only a single ASKAP FoV (comparable to our simulation of the GW170817 skymap in Figures 2 and 4). Such an event would have a final $\rho \gtrsim 60$ (at the time of the merger), corresponding to sources closer than $\sim$24 Mpc (Cannon et al. 2012), or a rate of $0.1^{+0.2}_{-0.1}$ yr^{-1} based on the BNS rate in Abbott et al. (2017b). Therefore, the prospects of seeing such an event during a year-long observing campaign are $\sim$0.1. For any realistic scenario, we will of course lose 60% of events to those detected below the ASKAP horizon, as well as $\sim$30% (assuming the alert for the event with small early-warning skymap is released 30 s before the merger) of the remaining events to those where the slew time is unacceptably long, meaning that we may only trigger on 12% of these very bright events. So we expect that ASKAP may be able to observe $\sim$0.012 events during O4. At least at radio wavelengths, we are not sensitive to weather and significantly less sensitive to day/night distinctions.

The discussion above focused on whether ASKAP could *observe* prompt emission but did not consider whether or not it could *detect* it. For that, we need to understand the flux density predictions of different models. Some models (e.g., Pshirkov & Postnov 2010; Hansen & Lyutikov 2001) predict that BNS mergers can produce FRB-like emission at low radio frequencies, $\lesssim$100 MHz, but this is too low for ASKAP, and some of them have a hard cut-off at the high frequency end (e.g., Wang et al. 2018). Moreover, no FRBs have been detected at those frequencies (e.g., Rowlinson et al. 2016; Chawla et al. 2017; Tingay et al. 2015; Sokolowski et al. 2018, although new detections are coming closer, Pilia et al. 2020; Chawla et al. 2020), which may influence the BNS/FRB rate comparison (e.g., Callister et al. 2016). Wang et al. (2016), Ravi & Lasky (2014) and Lyutikov (2013) predict the total power that can be emitted by BNS mergers. However, the flux

density at a given frequency is not clear. Instead, we parameterise this as $4\pi d^2 \nu S_\nu = xL$, where x depends on the spectrum of the emission and the upper and lower frequency limits. In Totani (2013), the signal is predicted to be $\sim$10^3 Jy at 24 Mpc, at a frequency of 888 MHz (assuming a radio emission efficiency of $\epsilon \sim 10^{-3}$, magnetic field strength of $B \sim 10^{12.5}$ G, neutron star radius of $R \sim 10$ km, and rotation periods of $P \sim 0.5$ ms). According to Table 2, if the merger follows the mechanism shown in Totani (2013), even with fly's eye mode ASKAP can detect the signal if covering the burst region. As mentioned above, BNSs within 24 Mpc are estimated to occur infrequently, at a rate of $0.1^{+0.2}_{-0.1}$ yr^{-1}. Though the expected flux density is high, the rate for such a bright event is low, which makes it harder to detect any prompt emission. For the other models, we could detect them if $x > 3 \times 10^{-6}$ (assuming a radio luminosity of $L \sim 10^{40}$ erg s^{-1} as in Wang et al. 2016, an event distance of $d \sim 24$ Mpc, and on observing frequency of 888 MHz).

In this paper, we have mainly focused on BNS mergers, although one of our sky maps in Figure 2 was actually from a neutron-star black-hole (NSBH) merger. We generally consider BNS mergers as more favourable to production of electromagnetic (EM) counterparts in general and FRB-like emission in particular, although Mingarelli, Levin & Lazio (2015) hypothesises that NSBH mergers could also produce FRBs. However, NSBH mergers will generally contain only a single magnetosphere and in many cases the NS will be swallowed by the BH without disruption (Mingarelli et al. 2015; Chatterjee et al. 2020), so many models for prompt emission will fail. Separately, NSBH mergers will generally be more distant (e.g., Abbott et al. 2019), leading to fainter EM emission, and the poorly constrained merger rate (Abbott et al. 2020) makes predictions difficult. Regardless, ASKAP still can and will search for the prompt emission from a well-localised NSBH merger, because the basic detection scenarios in terms of localisation will be similar to that for BNS mergers.

6. Conclusion

The detection of prompt emission from BNS mergers requires a radio instrument of sufficient sensitivity that is capable of being on-target before the arrival of a burst. In this paper, we estimated the probability for ASKAP to capture the prompt emission with negative-latency alerts from aLIGO/Virgo using two observational modes suitable for FRB-like emission. Fly's eye mode can achieve higher sky coverage but less sensitivity, while the collimated incoherent mode gains sensitivity at the expense of sky area. Given that faint, poorly localised events will also have minimal advance warning and so will not allow for sufficient slew times, it may be nearly impossible to capture any prompt emission from those events. However, brighter events will have both better advance warning and smaller localisations areas enabling more sensitive observations and more confident coverage of the whole localisation area: we can achieve better sensitivity (down to 3.2 Jy using all antennas incoherently with an 8σ detection threshold). If FRB-like emission can be detected from these events, we can get a more accurate localisation for the event (as small as $3'' \times 3''$ with more than three antennas with the same pointing), which can enable follow-up across the electromagnetic spectrum. While expected to be rare ($\sim$0.012 yr^{-1}), ASKAP observations of negative-latency triggers have the potential to discover prompt emission from BNS mergers or at least constrain their origin.

References

Aasi, J., et al. 2015, CQG, 32, 115012

Abbott, B. P., et al. 2017a, PhRvL, 119, 161101

Abbott, B. P., et al. 2017b, ApJ, 848, L13

Abbott, B. P., et al. 2018, LRvR, 21, 3

Abbott, B. P., et al. 2019, PhRvX, 9, 031040

Abbott, R., et al. 2020, ApJ, 896, L44

Acernese, F., et al. 2014, CQG, 32, 024001

Adams, T., et al. 2016, CQG, 33, 175012

Anderson, M. M., et al. 2018, ApJ, 864, 22

Aso, Y., Michimura, Y., Somiya, K., Ando, M., Miyakawa, O., Sekiguchi, T., Tatsumi, D., & Yamamoto, H. 2013, PhRvD, 88, 043007

Bannister, K. W., et al. 2017, ApJ, 841, L12

Bannister, K. W., et al. 2019, Sci, 365, 565

Bochenek, C. D., Ravi, V., Belov, K. V., Hallinan, G., Kocz, J., Kulkarni, S. R., & McKenna, D. L. 2020, Natur, submitted, arXiv:2005.10828

Callister, T., Kanner, J., & Weinstein, A. 2016, ApJ, 825, L12

Callister, T. A., et al. 2019, ApJ, 877, L39

Cannon, K., et al. 2012, ApJ, 748, 136

Cao, X.-F., Yu, Y.-W., & Zhou, X. 2018, ApJ, 858, 89

Chatterjee, D., Ghosh, S., Brady, P. R., Kapadia, S. J., Miller, A. L., Nissanke, S., & Pannarale, F. 2020, ApJ, 896, 54

Chawla, P., et al. 2017, ApJ, 844, 140

Chawla, P., et al. 2020, arXiv e-prints, in press, arXiv:2004.02862

Chu, Q., Howell, E. J., Rowlinson, A., Gao, H., Zhang, B., Tingay, S. J., Boër, M., & Wen, L., 2016, MNRAS, 459, 121

Cordes, J. M., & Chatterjee, S. 2019, ARA&A, 57, 417

Dal Canton, T., & Harry, I. W. 2017, arXiv e-prints, p. arXiv:1705.01845

Dobie, D., Murphy, T., Kaplan, D. L., Ghosh, S., Bannister, K. W., & Hunstead, R. W. 2019a, PASA, 36, e019

Dobie, D., et al. 2019b, ApJ, 887, L13

Fairhurst, S. 2009, NJPh, 11, 123006

Falcke, H., & Rezzolla, L. 2014, A&A, 562, A137

Hansen, B. M. S., & Lyutikov, M. 2001, MNRAS, 322, 695

Hooper, S., Chung, S. K., Luan, J., Blair, D., Chen, Y., & Wen, L. 2012a, PhRvD, 86, 024012

Hooper, S., et al. 2012b, JPhCS, 363, 012027

James, C. W., Anderson, G. E., Wen, L., Bosveld, J., Chu, Q., Kovalam, M., Slaven-Blair, T. J., & Williams, A. 2019b, MNRAS, 489, L75

James, C. W., Ekers, R. D., Macquart, J. P., Bannister, K. W., & Shannon, R. M. 2019a, MNRAS, 483, 1342

Johnston, S., et al. 2008, ExA, 22, 151

Kaplan, D. L., et al. 2015, ApJ, 814, L25

Kaplan, D. L., Murphy, T., Rowlinson, A., Croft, S. D., Wayth, R. B., & Trott, C. M. 2016, PASA, 33, e050

Lai, D. 2012, ApJ, 757, L3

LIGO Scientific Collaboration and Virgo Collaboration et al. 2019, GCN, 25324, 1

Lorimer, D. R., Bailes, M., McLaughlin, M. A., Narkevic, D. J., & Crawford, F. 2007, Sci, 318, 777

Lu, W., Kumar, P., & Narayan, R. 2019, MNRAS, 483, 359

Lu, W., & Piro, A. L. 2019, ApJ, 883, 40

Lyutikov, M. 2013, ApJ, 768, 63

Macquart, J. P., & Ekers, R. D. 2018, MNRAS, 474, 1900

Macquart, J.-P., et al. 2010, PASA, 27, 272–282

Margalit, B., Beniamini, P., Sridhar, N., & Metzger, B. D. 2020, ApJ, submitted, arXiv:2005.05283

Mereghetti, S., et al. 2020a, arXiv e-prints, p. arXiv:2005.06335

Mereghetti, S., Savchenko, V., Gotz, D., Ducci, L., Ferrigno, C., Bozzo, E., Borkowski, J., & Bazzano, A. 2020b, GRBCN, 27668, 1

Messick, C., et al. 2017, PhRvD, 95, 042001

Metzger, B. D., & Zivancev, C. 2016, MNRAS, 461, 4435

Mingarelli, C. M. F., Levin, J., & Lazio, T. J. W. 2015, ApJ, 814, L20

Nitz, A. H., Dal Canton, T., Davis, D., & Reyes, S. 2018, PhRvD, 98, 024050

Pilia, M., et al. 2020, ApJ, 896, L40

Pshirkov, M., & Postnov, K. 2010, Ap&SS, 330, 13

Ravi, V. 2019, NatAs, 3, 928

Ravi, V., & Lasky, P. D. 2014, MNRAS, 441, 2433

Ridnaia, A., et al. 2020a, arXiv e-prints, p. arXiv:2005.11178

Ridnaia, A., et al. 2020b, GRBCN, 27669, 1

Rowlinson, A., & Anderson, G. E. 2019, MNRAS, 489, 3316

Rowlinson, A., et al. 2016, MNRAS, 458, 3506

Sachdev, S., et al. 2019, PhRvD, submitted, arXiv:1901.08580

Scholz, P., & Chime/Frb Collaboration 2020, ATel, 13681, 1

Shannon, R. M., et al. 2018, Nature, 562, 386

Singer, L. P., & Price, L. R. 2016, PhRvD, PhRvD, 93, 024013

Singer, L. P., et al. 2014, ApJ, 795, 105

Sokolowski, M., et al. 2018, ApJ, 867, L12

Somiya, K. 2012, CQG, 29, 124007

Spitler, L. G., et al. 2016, Natur, 531, 202

Thornton, D., et al. 2013, Sci, 341, 53

Tingay, S. J., et al. 2013, PASA, 30, e007

Tingay, S. J., et al. 2015, AJ, 150, 199

Totani, T. 2013, PASJ, 65

Wang, J.-S., Peng, F.-K., Wu, K., & Dai, Z.-G. 2018, ApJ, 868, 19

Wang, J.-S., Yang, Y.-P., Wu, X.-F., Dai, Z.-G., & Wang, F.-Y. 2016, ApJ, 822, L7

Zhang, S. N., et al. 2020, ATel, 13687, 1